



Simulation of
GOES-R ABI aerosol
radiances using
WRF-CMAQ:

S. A. Christopher

Simulation of GOES-R ABI aerosol radiances using WRF-CMAQ: a case study approach

S. A. Christopher

Department of Atmospheric Science, University of Alabama in Huntsville, Huntsville, AL, USA

Received: 25 March 2013 – Accepted: 29 June 2013 – Published: 12 July 2013

Correspondence to: S. A. Christopher (sundar@nsstc.uah.edu)

Published by Copernicus Publications on behalf of the European Geosciences Union.

Title Page

Abstract

Introduction

Conclusions

References

Tables

Figures



Back

Close

Full Screen / Esc

Printer-friendly Version

Interactive Discussion



Abstract

The primary focus of this paper is to simulate visible and near-infrared reflectances of the GOES-R Advanced Baseline Imager (ABI) for cases of high aerosol loading containing regional haze and smoke over the eastern United States. The simulations are performed using the Weather Research and Forecasting (WRF), Sparse Matrix Operator Kernel Emissions (SMOKE), and Community Multiscale Air Quality (CMAQ) models. Geostationary satellite-derived biomass burning emissions are also included as an input to CMAQ. Using the CMAQ aerosol concentrations and Mie calculations, radiance is computed from the discrete ordinate atmospheric radiative transfer model. We present detailed methods for deriving aerosol extinction from WRF and CMAQ outputs. Our results show that the model simulations create a realistic set of reflectance in various aerosol scenarios. The simulated reflectance provides distinct spectral features of aerosols which is then compared to data from the Moderate Resolution Imaging Spectroradiometer (MODIS). We also present a simple technique to synthesize green band reflectance (which will not be available on the ABI), using the model-simulated blue and red band reflectance. This study is an example of the use of air quality modeling in improving products and techniques for Earth observing missions.

1 Introduction

The Geostationary Operational Environmental Satellites-R Series (GOES-R) is the next generation of geostationary satellites that will offer a continuation of current products and services and enable new and improved applications (Schmit et al., 2005). The Advanced Baseline Imager (ABI) on GOES-R (currently scheduled for 2015) will monitor clouds, aerosols, and surface features with a greater number of spectral bands and improved spatial resolutions (Schmit et al., 2008). The ABI will provide data in 16 spectral bands in the visible (0.47 and 0.64 μm), near-infrared (0.87, 1.38, 1.61, and 2.25 μm) and infrared (3.9, 6.19, 6.95, 7.34, 8.5, 9.61, 10.35, 11.2, 12.3 and 13.3 μm)

Simulation of GOES-R ABI aerosol radiances using WRF-CMAQ:

S. A. Christopher

Title Page

Abstract

Introduction

Conclusions

References

Tables

Figures



Back

Close

Full Screen / Esc

Printer-friendly Version

Interactive Discussion



portions of the electromagnetic spectrum. These improvements will help data assimilation and numerical weather prediction (NWP) applications, especially by providing crucial observations for regional and mesoscale data assimilations and predictions (Schmit et al., 2005).

5 Among the variety of application possibilities, GOES-R will also be used to monitor aerosols from fires and dust storms. The capabilities of GOES-R on air quality can currently be assessed by simulating what GOES-R ABI would see when it is in orbit. The synthetic radiance computations require inputs for meteorological and chemical species fields and could be obtained from air quality models (e.g., WRF-CMAQ or
10 WRF-CHEM).

To simulate radiance fields, we use the Discrete Ordinate Radiative Transfer model (Ricchiuzzi et al., 1998), to the existing CMAQ modeling system. This consists of three primary modeling components (Yang et al., 2011): the Weather Research and Forecasting model (WRF, version 3.2; Grell et al., 1995), Sparse Matrix Operator Kernel
15 Emissions model (SMOKE, version 2.5; Houyoux et al., 2000), and Community Multiscale Air Quality (CMAQ, version 4.6). The CMAQ model simulations include background emissions and fire emissions derived from satellites as described in Yang et al. (2011). The background emission rates are estimated using SMOKE with the 2002 National Emission Inventory (NEI). The WRF and CMAQ outputs are then used
20 as input to SBDART, which generates on-orbit radiance and reflectance at the GOES-R ABI bands.

This study examines the reflectance computed for three cases in the eastern United States for high aerosol loading events including haze and fires. The model-simulated RGB imagery is also compared with the Moderate Resolution Imaging Spectroradiometer (MODIS) data. We also compare the simulated surface $PM_{2.5}$ mass concentrations
25 with ground-based observations to assess the model performance. From the perspective of spectral signature of various features, we present a simple technique to synthesize green band reflectance, which will not be available on ABI. We show the synthetic

**Simulation of
GOES-R ABI aerosol
radiances using
WRF-CMAQ:**

S. A. Christopher

Title Page

Abstract

Introduction

Conclusions

References

Tables

Figures



Back

Close

Full Screen / Esc

Printer-friendly Version

Interactive Discussion



the measured surface PM_{2.5} quite well. The model performance for PM_{2.5} is consistent with the previous studies using the WRF-CMAQ and Eta-CMAQ over the eastern United States (Yu et al., 2012).

4.2 GOES-R reflectance

5 SBDART computes upward radiance and downward irradiance at the top of atmosphere (TOA). We convert them to reflectance for visualization (values from 0 to 1) and for interpretation purposes. Reflectance is defined as the ratio of the radiant flux reflected by a medium to that incident upon it. Therefore, spectral reflectance at TOA is given by

$$10 R_{\lambda} = (\pi \cdot I_{\lambda}) / (F_{\lambda} \cdot \cos \theta)$$

where R_{λ} , I_{λ} , and F_{λ} are spectral reflectance (unitless), spectral radiance ($\text{W m}^{-2} \mu\text{m}^{-1} \text{sr}^{-1}$), and spectral irradiance of the sun ($\text{W m}^{-2} \mu\text{m}^{-1}$) at TOA, respectively. The quantity $(\pi \cdot I_{\lambda})$ represents total upward radiant flux and θ denotes the solar zenith angle ($^{\circ}$). Since the ABI filters reduce the apparent scene radiance and solar flux, reflectance should be unfiltered to produce the reflectance measured by GOES-R ABI at TOA. The unfiltered ABI spectral reflectance is computed as

$$15 R\lambda = \frac{\pi \cdot \int_{\lambda_1}^{\lambda_2} S\lambda I\lambda d\lambda}{\cos \theta \cdot \int_{\lambda_1}^{\lambda_2} S\lambda F\lambda d\lambda},$$

where S_{λ} is the spectral response of each ABI band. λ_1 and λ_2 are the cutoff wavelengths beyond which filter response is assumed zero. We set the cutoff wavelengths at $\lambda_0 \pm 0.5 \cdot \text{FWHM}$, where λ_0 and FWHM are the central wavelength and full width at half maximum. The spectral response is assumed as Gaussian Boxcar Hybrid (GBH), where the top of the curve is flattened out (data available at ftp://ftp.ssec.wisc.edu/ABI/SRF). However, the actual instrument response function should be determined after the launch of GOES-R.

Simulation of GOES-R ABI aerosol radiances using WRF-CMAQ:

S. A. Christopher

Title Page

Abstract

Introduction

Conclusions

References

Tables

Figures

◀

▶

◀

▶

Back

Close

Full Screen / Esc

Printer-friendly Version

Interactive Discussion



true color imageries because of the difference in viewing geometry between MODIS and GOES-R.

The cloud, aerosol, land, and ocean are well simulated in these images in Fig. 4 although there is a need for improved cloud representation in dynamical models. The clouds often differ from their positions in the simulated images due to difficulty in simulating the observed clouds from WRF. The model does not reproduce the small scale convective clouds during summer, especially on 8 July 2010 which is a topic for further investigation. The smoke aerosols on 10 June 2008 (Fig. 1, left) are spread more evenly along the mid-Atlantic coast (Fig. 4, left). This also happens to the plumes from the wildfires in the southern Georgia simulations on 25 March 2011, where plumes at two separate locations (Fig. 1, right) are viewed as one combined plume in the simulation (Fig. 4, right). The simulated haze on 8 July 2010 is seen in the eastern states (Fig. 4, middle), where the haze in Illinois, Indiana, and Kentucky was not apparent because of cloud in Fig. 1 (middle). It is shown that the simulations can capture the ocean color in the coastline of the Bahamas and around Key West. The model simulations are at 12 km spatial resolution where the surface consists of different land use types such as water, soil, trees, grasses, and so on. Thus, the simulated land surface scene may represent the mixture of different land use.

5 Synthetic RGB imagery

The GOES-R ABI does not contain a green band. However, because the green band is essential to produce RGB true-color imagery, we develop and demonstrate a technique to derive the green band reflectance from other ABI bands. This section starts by showing spectral signatures of various features at the ABI visible and near-IR bands and then shows how the reflectance in the green band can be calculated by using the red and blue bands, keeping in mind that this is only an approximation.

Simulation of GOES-R ABI aerosol radiances using WRF-CMAQ:

S. A. Christopher

Title Page

Abstract

Introduction

Conclusions

References

Tables

Figures



Back

Close

Full Screen / Esc

Printer-friendly Version

Interactive Discussion



green and near-IR light than the stressed vegetation, the stressed vegetation and soil would have increasing reflectance with increasing wavelength. The spectral signature for land in Fig. 5 shows that the reflectance at the red band is slightly higher than at the green band, indicating the healthy vegetation is not the major contributor to reflectance spectra at the 12 km spatial resolution in this study.

5.2 Synthetic green band reflectance

The green band can be approximated using a look-up-table (LUT) approach, either using the MODIS blue, red, and near-IR bands (Miller et al., 2012) or using the blue, red, and near-IR band simulations from a radiative transfer model (Hillger et al., 2011). Both these approaches indicate that the synthesized green band imagery agrees with the observed MODIS or simulated green, reporting a less-green bias in the synthesized green values.

Miller et al. (2012) assume that the green band reflectance for each scene is a function of the red, blue, and near-IR (0.86 μm) bands. They generate scene-dependent green band LUTs from the MODIS red, blue, and near-IR bands. Once the ABI red, blue, and near-IR band reflectance were given, the green band reflectance is selected for the pair of the red-blue-near IR reflectance that makes the best match between the MODIS and ABI. This LUT approach would produce the MODIS green band reflectance, not the GOES-R ABI reflectance. We expect slightly different spectral signatures of scenes between the MODIS and ABI because the MODIS and ABI have different filter spectral response and viewing geometries.

In contrast, Hillger et al. (2011) compute radiances at 0.47 μm (blue), 0.64 μm (red), and 0.865 μm (near-IR) using a radiative transfer model along with the regional atmospheric modeling system (RAMS) outputs and the MODIS surface albedo product. The green band imagery is approximated from the blue, red, near-IR band simulations using the LUT method and compared with the directly-simulated green band imagery.

Our study study uses a set of models (WRF, SMOKE, CMAQ, and SBDART) that enables description of the “realistic” state of land surface, ocean, and atmosphere. As

Simulation of GOES-R ABI aerosol radiances using WRF-CMAQ:

S. A. Christopher

Title Page

Abstract

Introduction

Conclusions

References

Tables

Figures

⏪

⏩

◀

▶

Back

Close

Full Screen / Esc

Printer-friendly Version

Interactive Discussion



**Simulation of
GOES-R ABI aerosol
radiances using
WRF-CMAQ:**

S. A. Christopher

Title Page

Abstract

Introduction

Conclusions

References

Tables

Figures

◀

▶

◀

▶

Back

Close

Full Screen / Esc

Printer-friendly Version

Interactive Discussion



a result, it is possible to investigate the spectral reflectance relationships in complex scenes. We introduce five distinctive classes in the model domain, which are classified as land, ocean, aerosol, cloud, and “coastline”. The aerosol and cloud are further separated into two classes in Table 2. For example, aerosols over land and ocean show different spectral behavior because coarse mode particles (dominated by sea salt) increase over ocean. Similarly, liquid cloud is distinguished from ice cloud due to the differences in the imaginary part of their refractive index. Figure 6 shows the ice cloud can be discriminated from the liquid cloud using the visible ($0.55\ \mu\text{m}$ or $0.64\ \mu\text{m}$), and near-IR ($1.38\ \mu\text{m}$ or $1.61\ \mu\text{m}$) (e.g., Schmidt et al., 2005; Baum et al., 2005).

This study focuses on synthesizing the green band reflectance as a function of reflectance at visible and near-IR bands. Figure 6 shows the relationships between the green and other band reflectance for each class. As expected, the classes show complex spectral responses of reflectance. Surprisingly, strong linear relationships are found between $R_{0.47\ \mu\text{m}}$ and $R_{0.55\ \mu\text{m}}$ (top left in Fig. 6) and between $R_{0.64\ \mu\text{m}}$ and $R_{0.55\ \mu\text{m}}$ (top middle in Fig. 6) for all classes specified in Table 2, where $R_{0.47\ \mu\text{m}}$, $R_{0.55\ \mu\text{m}}$, and $R_{0.64\ \mu\text{m}}$ are reflectance in the blue, green, and red bands, respectively. The high correlation between $R_{0.47\ \mu\text{m}}$ and $R_{0.55\ \mu\text{m}}$ and between $R_{0.64\ \mu\text{m}}$ and $R_{0.55\ \mu\text{m}}$ indicates that the blue, green, and red bands contain redundant spectral information for certain classes. We expect that $R_{0.55\ \mu\text{m}}$ in a pixel can be predicted (or synthesized) by $R_{0.47\ \mu\text{m}}$ and $R_{0.64\ \mu\text{m}}$.

5.3 RGB imagery

A linear relationship between $R_{0.55\ \mu\text{m}}$ and $R_{0.64\ \mu\text{m}}$ (and between $R_{0.55\ \mu\text{m}}$ and $R_{0.47\ \mu\text{m}}$) is not sufficient enough to derive $R_{0.55\ \mu\text{m}}$ from $R_{0.64\ \mu\text{m}}$ because the linear relationship differs from one class to another. Therefore, it is necessary to classify each scene before applying the linear relationship although scene classification could be a challenging problem. Alternatively, it is noted in Fig. 6 that green band reflectance can be approximated by one or two linear combinations of blue and red band reflectance for all classes.

Simulation of GOES-R ABI aerosol radiances using WRF-CMAQ:

S. A. Christopher

Title Page

Abstract

Introduction

Conclusions

References

Tables

Figures

⏪

⏩

◀

▶

Back

Close

Full Screen / Esc

Printer-friendly Version

Interactive Discussion

The green band reflectance can be expressed as a simple relation, $G_{\text{syn}} = w_B \cdot B + w_R \cdot R$, where G_{syn} , B , and R are the synthesized green, simulated red, and simulated blue band reflectance, respectively. The coefficients, w_B and w_R , give the weights of blue and red band reflectance in determining green band reflectance. However, w_B and w_R differ for different classes, but w_B and w_R have a range within which the synthesized green band reflectance is close to the simulated one for all classes. Figure 7 shows the difference between the actual (simulated) and synthesized green band reflectance, where the synthesized reflectance is derived by $G_{\text{syn}} = w_B \cdot B + w_R \cdot R$ with varying w_B and w_R . Since the minima of reflectance difference occur over a range, not at a point, in w_B and w_R space, we can select an optimal weight pair whose reflectance difference is close to minimum for all classes.

After searching for optimal w_B and w_R pairs for three different days, we chose two w_B and w_R pairs such that green band reflectance is well approximated (synthesized) by the relations,

$$G_{\text{syn}} = 0.4 \cdot B + 0.6 \cdot R \quad \text{for land, ocean, aerosol, and cloud}$$

$$G_{\text{syn}} = 0.6 \cdot B + 0.6 \cdot R \quad \text{for coastline}$$

Figure 8 shows that the synthesized (G_{syn}) and simulated green band reflectance (G) are almost the same except for coastline. The relatively large uncertainty in G_{syn} for coastline was also recognized in the LUT method (Hillger et al., 2011; Miller et al., 2012). The synthesized green band reflectance differs from the simulated by up to about 0.01 for land, ocean, aerosol, and cloud and by 0.01–0.03 for coastline.

The synthetic RGB imagery using the synthetic green band reflectance is shown in Fig. 9. The synthetic RGB imagery appears almost identical to the simulated one with subtle biases. The ocean and cloud in the synthesized RGB imagery (Fig. 8) are slightly brighter (less than 0.01 in reflectance) than those in the simulated RGB imagery (Fig. 4).

We introduce an approach to synthesize RGB imagery while there is a missing green band in GOES-R ABI. This approach uses the synthesized green band re-

Simulation of GOES-R ABI aerosol radiances using WRF-CMAQ:

S. A. Christopher

Title Page

Abstract

Introduction

Conclusions

References

Tables

Figures

⏪

⏩

◀

▶

Back

Close

Full Screen / Esc

Printer-friendly Version

Interactive Discussion

flectance that is derived by a simple relation of the red and blue band reflectance, i.e., $G_{\text{syn}} = 0.4 \cdot B + 0.6 \cdot R$. Since the coastline occurs at fixed locations, we can apply the same linear equation and then add $0.2 \cot B$ to the pre-defined coastline to synthesize the green band reflectance for coastline. The correction factor for coastline, $0.2 \cot B$, can be obtained from the MODIS 16 day albedo product that provides the atmospherically corrected, cloud-cleared reflectances (Schaaf et al., 2002). It is also possible to apply the equation, $G_{\text{syn}} = 0.4 \cot B + 0.6 \cot R$, to all classes although this simplest approach may cause a little more bias in coastline. The difference is probably negligible considering the reflectance difference for coastline in Fig. 7 at $w_B = 0.4$ and 0.6 . The approach shown in this study is attractive for operational purposes because it produces RGB imagery well, needs only simple calculations, and does not need a database for LUTs.

6 Summary and discussion

The GOES-R ABI visible and near-infrared reflectance are simulated using WRF, SMOKE, CMAQ, and SBDART models for cases of high aerosol loadings with haze and smoke over the eastern United States. The simulations reproduce the state of meteorological fields, background emissions, and chemical transport of air pollutants. To represent more realistic scenarios, satellite-derived biomass burning emissions are also included as an input to CMAQ. The simulated RGB imagery appears realistic in various aerosol scenarios. We classify the model scenes by seven classes based on their spectral signatures at the 12 km spatial resolution. The green band reflectance is synthesized from red and blue bands. The resulting synthesized RGB images appear almost identical to the model-simulated ones.

This study examines the use of air quality modeling to simulate spectral signatures from various scenes. We show that the model-based spectral signatures provide a simple way to select relevant and to deselect irrelevant spectral information from multi-spectral data. As an exercise, we synthesize true color imagery which perhaps ap-

Simulation of GOES-R ABI aerosol radiances using WRF-CMAQ:

S. A. Christopher

Title Page

Abstract

Introduction

Conclusions

References

Tables

Figures

◀

▶

◀

▶

Back

Close

Full Screen / Esc

Printer-friendly Version

Interactive Discussion

5. Q_{ext} , the Mie extinction efficiency factor, is a function of α and index of refraction of the particles. It is calculated from the Evans and Fournier approximation (Evans and Fournier, 1990) for each CMAQ species.
6. The aerosol extinction coefficient b_{sp} (km^{-1}) must be calculated from ambient aerosol characteristics as index of refraction ($m = n - ik$), volume concentration and size distribution; at wavelength λ , b_{sp} (km^{-1}) may be expressed as (Binkowski and Roselle, 2003):

$$\beta_{\text{sp}} = \frac{3\pi}{2\lambda} \int_{-\infty}^{\infty} \frac{Q_{\text{ext}}}{\alpha} \frac{dV}{d\ln\alpha} d\ln\alpha$$

The particle distribution is given in a lognormal form as

$$\frac{dV}{d\ln\alpha} = V_T \left(\frac{A}{\pi}\right)^{1/2} \exp\left[-A\ln^2\left(\frac{\alpha}{\alpha_v}\right)\right]$$

where $\alpha = \frac{\pi D}{\lambda}$, $\alpha_v = \frac{\pi D_g}{\lambda}$, and $A = \frac{1}{2\ln^2\sigma_g}$. V_T is the total particle volume concentration, and Q_{ext} , the Mie extinction efficiency factor as mentioned above.

If the water uptake effect is included, i.e., ambient environments are considered, the above equation becomes,

$$\begin{aligned} \beta_{\text{sp}} &= \frac{3\pi}{2\lambda} \int_{-\infty}^{\infty} \frac{Q_{\text{ext, amb}}}{\alpha_{\text{amb}}} \frac{dV_{\text{amb}}}{d\ln\alpha_{\text{amb}}} d\ln\alpha_{\text{amb}} = \frac{3\pi}{2\lambda} \int_{-\infty}^{\infty} \frac{Q_{\text{ext, amb}}}{\alpha_{\text{dry}}} \cdot g(\text{RH})^2 \cdot \frac{dV_{\text{dry}}}{d\ln\alpha_{\text{dry}}} d\ln\alpha_{\text{dry}} \\ &= \frac{3\pi}{2\lambda} \cdot g(\text{RH})^2 \cdot V_{\text{dry}} \cdot \left(\frac{1}{2\pi\ln^2\sigma_g}\right)^{(1/2)} \cdot \int_0^{\infty} \frac{Q_{\text{ext, amb}}}{\alpha^2} \cdot \exp\left[-\frac{1}{2} \cdot \frac{\ln^2\left(\frac{\alpha}{\alpha_v}\right)}{\ln^2\sigma_g}\right] \cdot d\alpha \end{aligned}$$

Simulation of GOES-R ABI aerosol radiances using WRF-CMAQ:

S. A. Christopher

Title Page

Abstract

Introduction

Conclusions

References

Tables

Figures

⏪

⏩

◀

▶

Back

Close

Full Screen / Esc

Printer-friendly Version

Interactive Discussion

- Binkowski, F. S. and Roselle, S. J.: Models-3 Community Multiscale Air Quality (CMAQ) model aerosol component 1. Model description, *J. Geophys. Res. Atm.*, 108, 4183, doi:10.1029/2001jd001409, 2003.
- Evans, B. T. N. and Fournier, G. R.: Simple approximation to extinction efficiency valid over all size parameters, *Appl. Optics*, 29, 4666–4670, 1990.
- 5 Grell, G. A., Dudhia, J., and Stauffer, D. R.: A description of the Fifth-Generation Penn State/NCAR Mesoscale Model (MM5), NCAR Technical Note, NCAR/TN 398+STR, Boulder, CO, 138, 1995.
- Hess, M., Koepke, P., and Schult, I.: Optical properties of aerosols and clouds: the software package OPAC, *B. Am. Meteorol. Soc.*, 79, 831–844, doi:10.1175/1520-0477(1998)079<0831:OPOAAC>2.0.CO;2, 1998.
- 10 Hillger, D., Grasso, L., Miller, S., Brummer, R., and DeMaria, R.: Synthetic advanced baseline imager true-color imagery, *J. Appl. Remote. Sens.*, 5, 053520, doi:10.1117/1.3576112, 2011.
- Houyoux, M. R., Vukovich, J. M., Coats Jr., C. J., Wheeler, N. J. M., and Kasibhatla, P. S.: Emission inventory development and processing for the Seasonal Model for Regional Air Quality (SMRAQ) project, *J. Geophys. Res.-Atmos.*, 105, 9079–9090, 2000.
- 15 Miller, S. D., Schmidt, C. C., Schmit, T. J., and Hillger, D. W.: A case for natural colour imagery from geostationary satellites, and an approximation for the GOES-R ABI, *Int. J. Remote Sens.*, 33, 3999–4028, 2012.
- 20 Ricchiazzi, P., Yang, S., Gautier, C., and Sowle, D.: SBDART: A research and teaching software tool for plane-parallel radiative transfer in the earth's atmosphere, *B. Am. Meteorol. Soc.*, 79, 2101–2114, 1998.
- Schaaf, C. B., Gao, F., Strahler, A. H., Lucht, W., Li, X., Tsang, T., Strugnell, N. C., Zhang, X., Jin, Y., Muller, J.-P., Lewis, P., Barnsley, M., Hobson, P., Disney, M., Roberts, G., Dunderdale, M., Doll, C., d'Entremont, R. P., Hu, B., Liang, S., Privette, J. L., and Roy, D.: First operational BRDF, albedo nadir reflectance products from MODIS, *Remote Sens. Environ.*, 83 135–148, doi:10.1016/s0034-4257(02)00091-3, 2002.
- 25 Schmit, T. J., Gunshor, M. M., Menzel, W. P., Gurka, J. J., Li, J., and Bachmeier, A. S.: Introducing the next-generation advanced baseline imager on GOES-R, *B. Am. Meteorol. Soc.*, 86, 1079–1096, 2005.
- 30 Schmit, T. J., Li, J., Gurka, J. J., Goldberg, M. D., Schrab, K. J., Li, J., and Feltz, W. F.: The GOES-R advanced baseline imager and the continuation of current sounder products, *J. Appl. Meteorol. Clim.*, 47, 2696–2711, 2008.

Simulation of GOES-R ABI aerosol radiances using WRF-CMAQ:

S. A. Christopher

Title Page

Abstract

Introduction

Conclusions

References

Tables

Figures

⏪

⏩

◀

▶

Back

Close

Full Screen / Esc

Printer-friendly Version

Interactive Discussion



Stamnes, K., Tsay, S. C., Wiscombe, W., and Jayaweera, K.: Numerically stable algorithm for discrete-ordinate-method radiative transfer in multiple scattering and emitting layered media, *Appl. Optics*, 27, 2502–2509, 1988.

Vermote, E. F., Tanré, D., Deuzé, J. L., Herman, M., and Morcrette, J. J.: Second simulation of the satellite signal in the solar spectrum, 6s: an overview, *IEEE T. Geosci. Remote*, 35, 675–686, 1997.

Yang, E.-S., Christopher, S. A., Kondragunta, S., and Zhang, X.: Use of hourly Geostationary Operational Environmental Satellite (GOES) fire emissions in a Community Multiscale Air Quality (CMAQ) model for improving surface particulate matter predictions, *J. Geophys. Res.*, 116, D04303, doi:10.1029/2010jd014482, 2011.

Yu, S., Mathur, R., Schere, K., Kang, D., Pleim, J., Young, J., Tong, D., Pouliot, G., McKeen, S. A., and Rao, S. T.: Evaluation of real-time PM_{2.5} forecasts and process analysis for PM_{2.5} formation over the eastern United States using the Eta-CMAQ forecast model during the 2004 ICARTT study, *J. Geophys. Res.-Atmos.*, 113, D06204, doi:10.1029/2007JD009226, 113, 2008.

Yu, S., Mathur, R., Pleim, J., Pouliot, G., Wong, D., Eder, B., Schere, K., Gilliam, R., and Rao, S. T.: Comparative evaluation of the impact of WRF/NMM and WRF/ARW meteorology on CMAQ simulations for PM_{2.5} and its related precursors during the 2006 TexAQS/GoMACCS study, *Atmos. Chem. Phys.*, 12, 4091–4106, doi:10.5194/acp-12-4091-2012, 2012.

Simulation of GOES-R ABI aerosol radiances using WRF-CMAQ:

S. A. Christopher

Title Page	
Abstract	Introduction
Conclusions	References
Tables	Figures
◀	▶
◀	▶
Back	Close
Full Screen / Esc	
Printer-friendly Version	
Interactive Discussion	

Table 1. Inputs and configurations.

	WRF	SMOKE	CMAQ
Horizontal	12 km × 12 km	12 km × 12 km	12 km × 12 km
Vertical	21 layers	1 and 15 ^a layers	21 layers
Input	RUC	NEI 2002	WRF output SMOKE emissions Fire emissions
Option	Kain-Fritsch (cu.) WSM-6 class (cloud) RRTM/Dudhia (rad.) YSU (PBL) Noah (land sfc)		CB-IV (gas-phase) AE4 (aerosol) AQ (aqueous/cloud)

^a Point emission sources.



Simulation of GOES-R ABI aerosol radiances using WRF-CMAQ:

S. A. Christopher

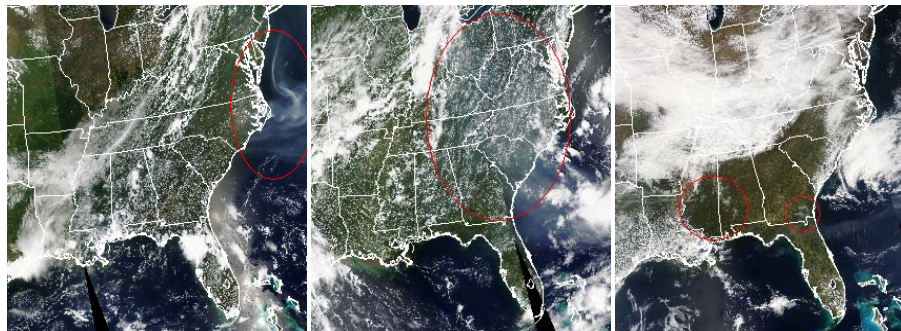


Fig. 1. MODIS Aqua imagery shows smoke from the Evans Road fire in North Carolina on 10 June 2008 (left), haze in Ohio Valley and Southeast on 8 July 2010 (middle), and agricultural fires and wildfires in Louisiana, Mississippi, Alabama, Georgia, and Florida on 25 March 2011 (right). The areas covered by plumes are shown as the red ovals. The imagery is available from <http://www.star.nesdis.noaa.gov>.

[Title Page](#)[Abstract](#)[Introduction](#)[Conclusions](#)[References](#)[Tables](#)[Figures](#)[Back](#)[Close](#)[Full Screen / Esc](#)[Printer-friendly Version](#)[Interactive Discussion](#)

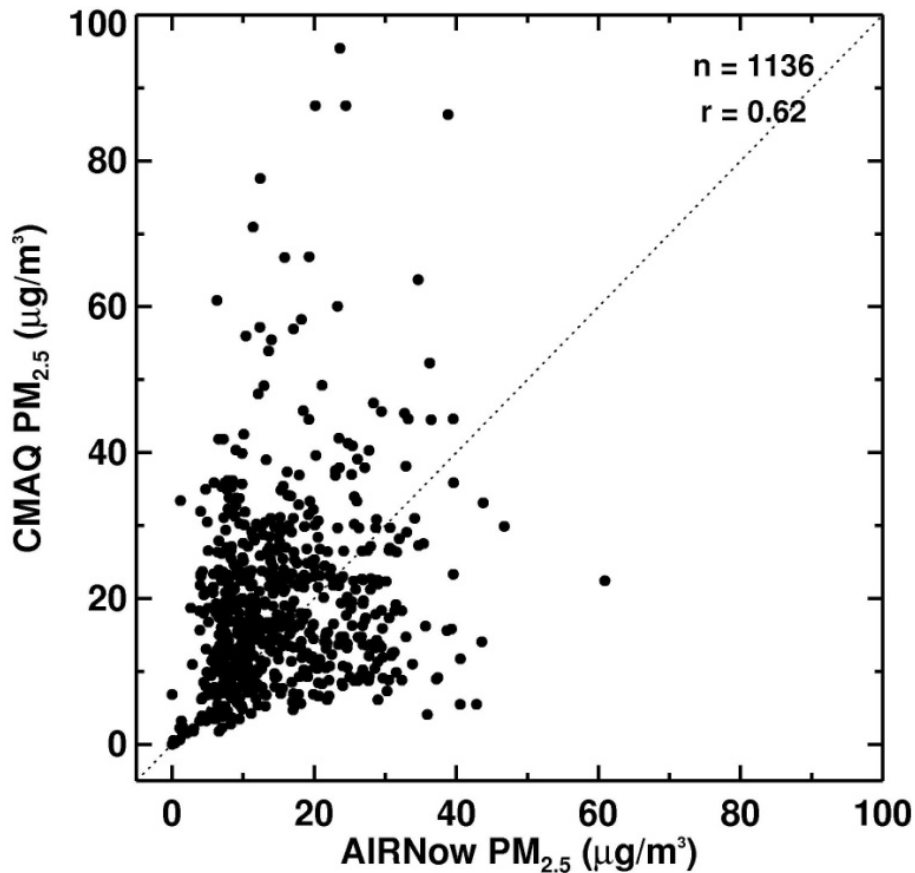


Fig. 2. Comparison of the simulated daily PM_{2.5} mass concentrations with the measured at the AIRNow stations for 10 June 2008, 8 July 2010, and 25 March 2011.

Simulation of
GOES-R ABI aerosol
radiances using
WRF-CMAQ:

S. A. Christopher

Title Page	
Abstract	Introduction
Conclusions	References
Tables	Figures
◀	▶
◀	▶
Back	Close
Full Screen / Esc	
Printer-friendly Version	
Interactive Discussion	



Simulation of GOES-R ABI aerosol radiances using WRF-CMAQ:

S. A. Christopher

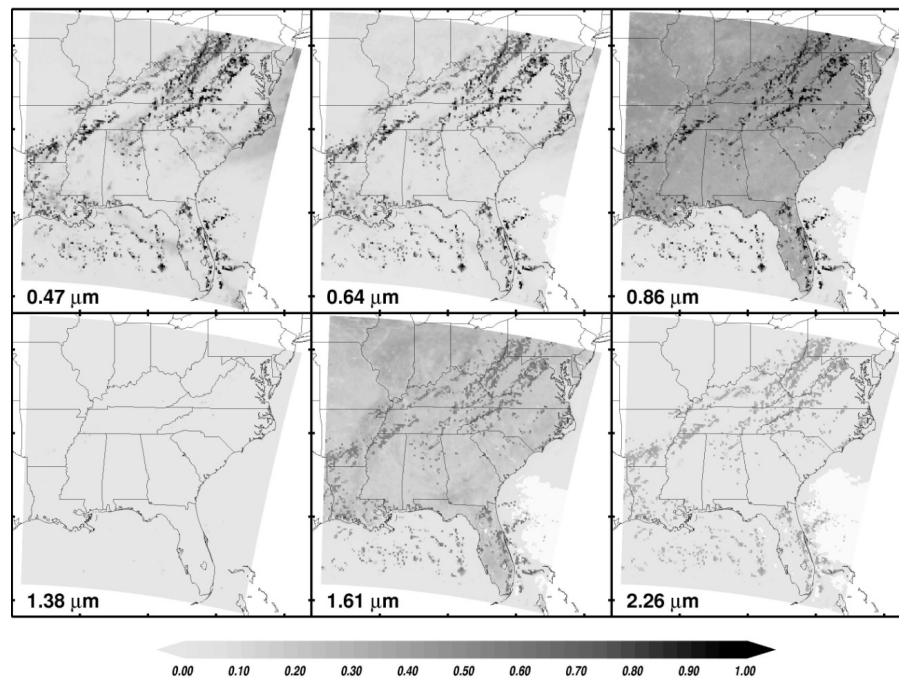
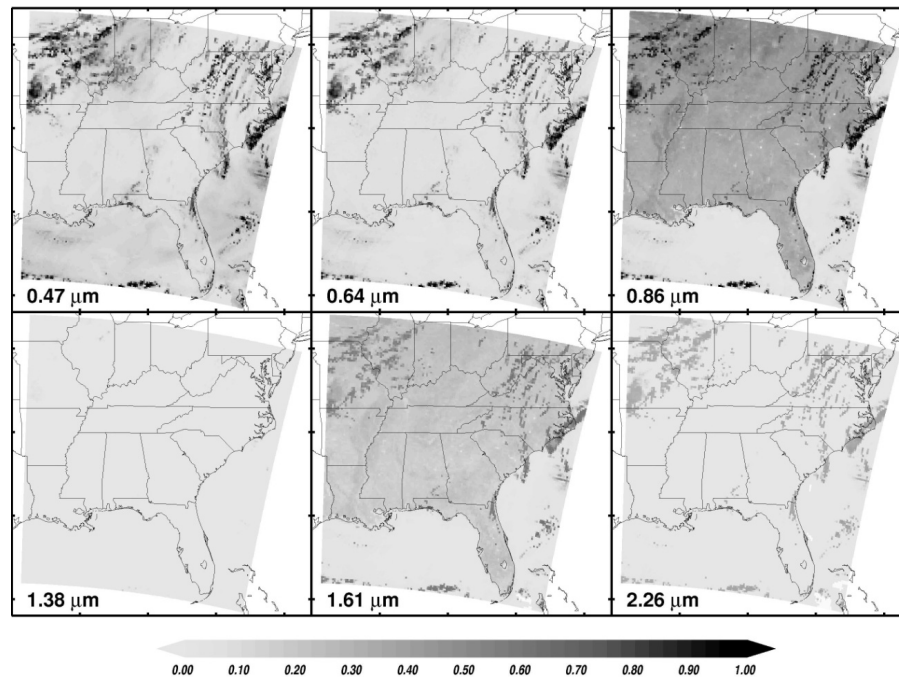


Fig. 3a. Model-simulated ABI reflectance for visible (0.47 and 0.64 μm), near-IR (0.87, 1.38, 1.61, and 2.25 μm) bands on 10 June 2008. Note the reflectance range is all from zero to one.

[Title Page](#)[Abstract](#)[Introduction](#)[Conclusions](#)[References](#)[Tables](#)[Figures](#)[◀](#)[▶](#)[◀](#)[▶](#)[Back](#)[Close](#)[Full Screen / Esc](#)[Printer-friendly Version](#)[Interactive Discussion](#)

**Simulation of
GOES-R ABI aerosol
radiances using
WRF-CMAQ:**

S. A. Christopher

**Fig. 3b.** Same as in Fig. 3a, but on 8 July 2010.[Title Page](#)[Abstract](#)[Introduction](#)[Conclusions](#)[References](#)[Tables](#)[Figures](#)[◀](#)[▶](#)[◀](#)[▶](#)[Back](#)[Close](#)[Full Screen / Esc](#)[Printer-friendly Version](#)[Interactive Discussion](#)

**Simulation of
GOES-R ABI aerosol
radiances using
WRF-CMAQ:**

S. A. Christopher

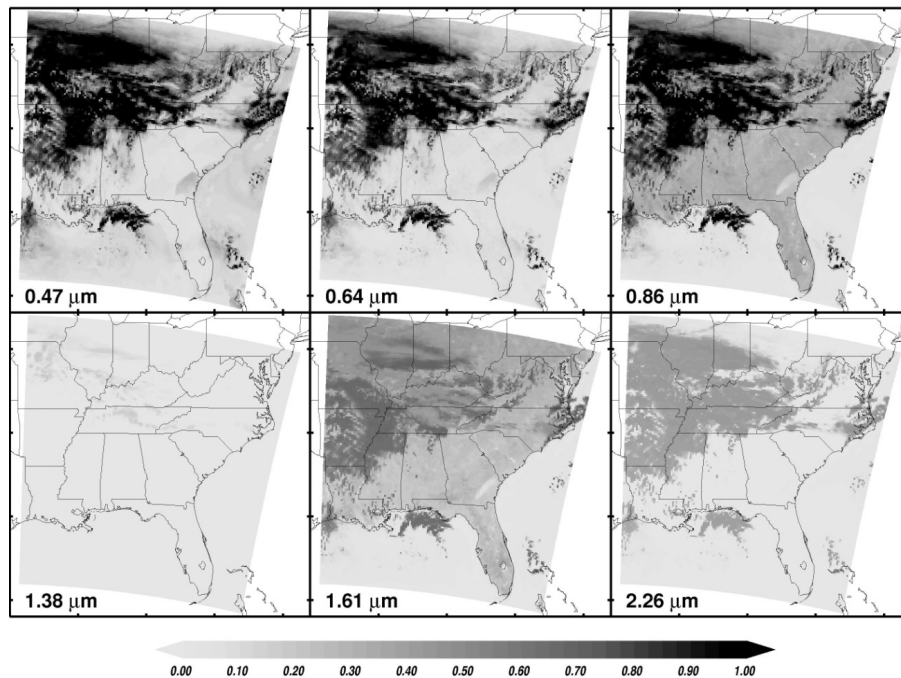


Fig. 3c. Same as in Fig. 3a, but on 25 March 2011.

Title Page

Abstract

Introduction

Conclusions

References

Tables

Figures

◀

▶

◀

▶

Back

Close

Full Screen / Esc

Printer-friendly Version

Interactive Discussion



Simulation of GOES-R ABI aerosol radiances using WRF-CMAQ:

S. A. Christopher

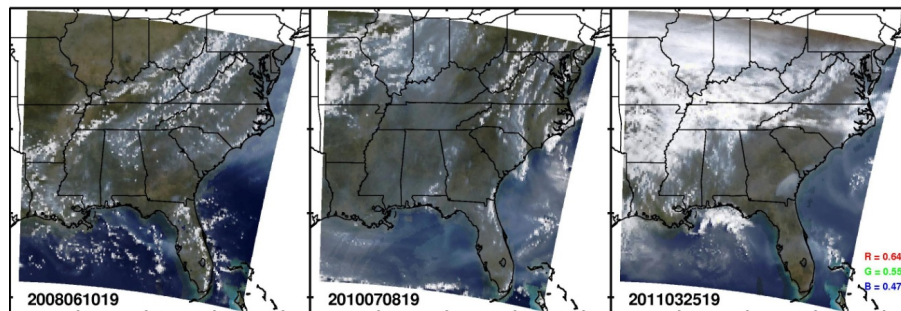


Fig. 4. The simulated RGB imagery viewed from GOES-R on 10 June 2008 (left), 8 July 2010 (middle), and 25 March 2011 (right). The images are enhanced using the image enhancement algorithm of the MODIS rapid response system.

[Title Page](#)[Abstract](#)[Introduction](#)[Conclusions](#)[References](#)[Tables](#)[Figures](#)[⏪](#)[⏩](#)[◀](#)[▶](#)[Back](#)[Close](#)[Full Screen / Esc](#)[Printer-friendly Version](#)[Interactive Discussion](#)

Simulation of
GOES-R ABI aerosol
radiances using
WRF-CMAQ:

S. A. Christopher

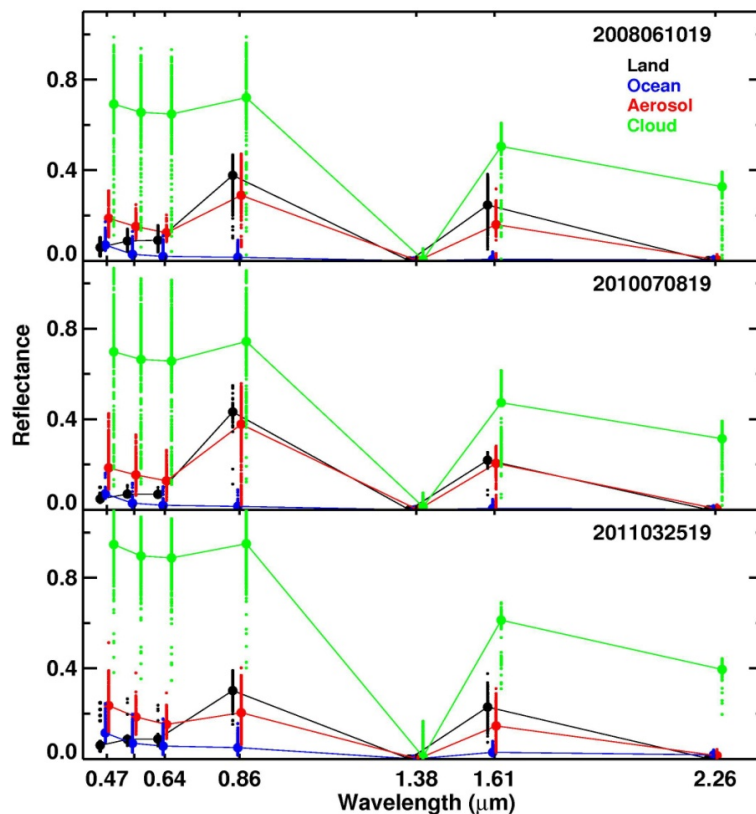


Fig. 5. Spectral signatures of land, ocean, aerosol, and cloud for 10 June 2008 (top), 8 July 2010 (middle), and 25 March 2011 (bottom). The spectral signatures for the imaginary green band are also shown between the blue and red bands.

[Title Page](#)[Abstract](#)[Introduction](#)[Conclusions](#)[References](#)[Tables](#)[Figures](#)[◀](#)[▶](#)[◀](#)[▶](#)[Back](#)[Close](#)[Full Screen / Esc](#)[Printer-friendly Version](#)[Interactive Discussion](#)

Simulation of GOES-R ABI aerosol radiances using WRF-CMAQ:

S. A. Christopher

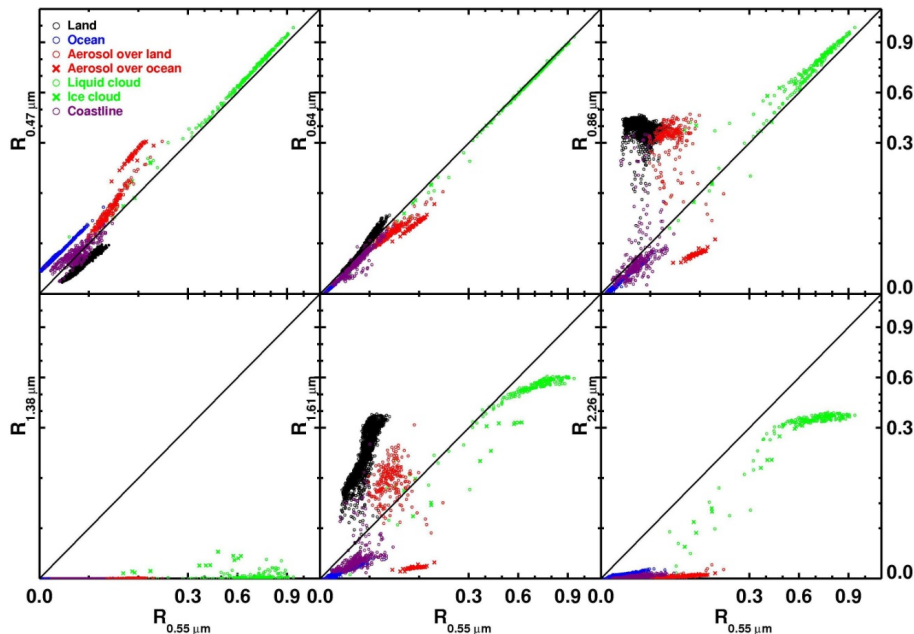


Fig. 6a. Plot of reflectance at the visible and near-IR bands against reflectance at the green band at 19:00 UTC, 10 June 2008. The Spectral signatures are shown for land, ocean, aerosol (over land and ocean), cloud (water and ice), and coastline. Note that the reflectance interval of 0.0 to 0.3 is enlarged to show more details of signatures from land, ocean, aerosol, and coastline.

[Title Page](#)
[Abstract](#)
[Introduction](#)
[Conclusions](#)
[References](#)
[Tables](#)
[Figures](#)
[⏪](#)
[⏩](#)
[⏴](#)
[⏵](#)
[Back](#)
[Close](#)
[Full Screen / Esc](#)
[Printer-friendly Version](#)
[Interactive Discussion](#)

Simulation of GOES-R ABI aerosol radiances using WRF-CMAQ:

S. A. Christopher

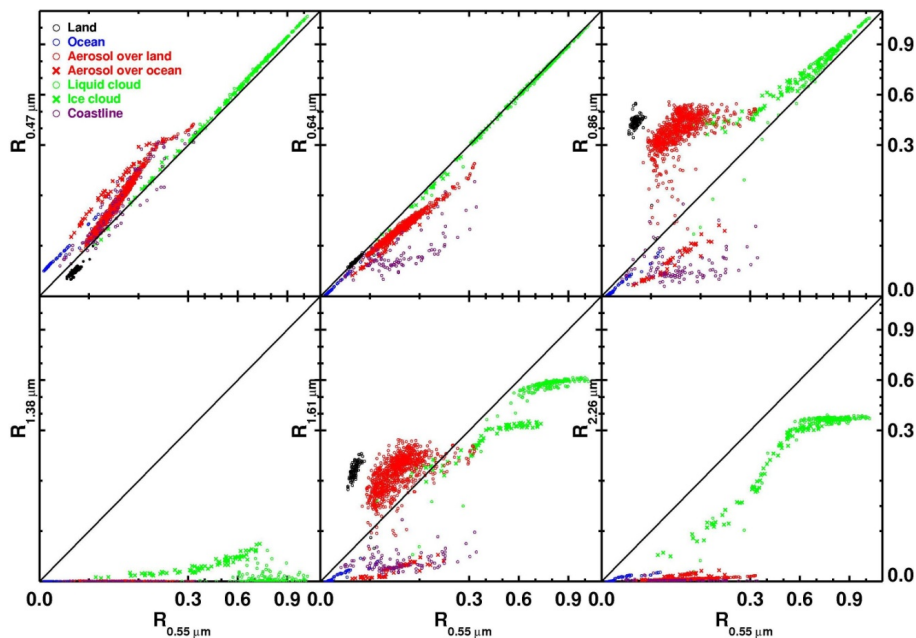


Fig. 6b. Same as in Fig. 6a, but on 8 July 2010.

Title Page

Abstract

Introduction

Conclusions

References

Tables

Figures

◀

▶

◀

▶

Back

Close

Full Screen / Esc

Printer-friendly Version

Interactive Discussion

Simulation of GOES-R ABI aerosol radiances using WRF-CMAQ:

S. A. Christopher

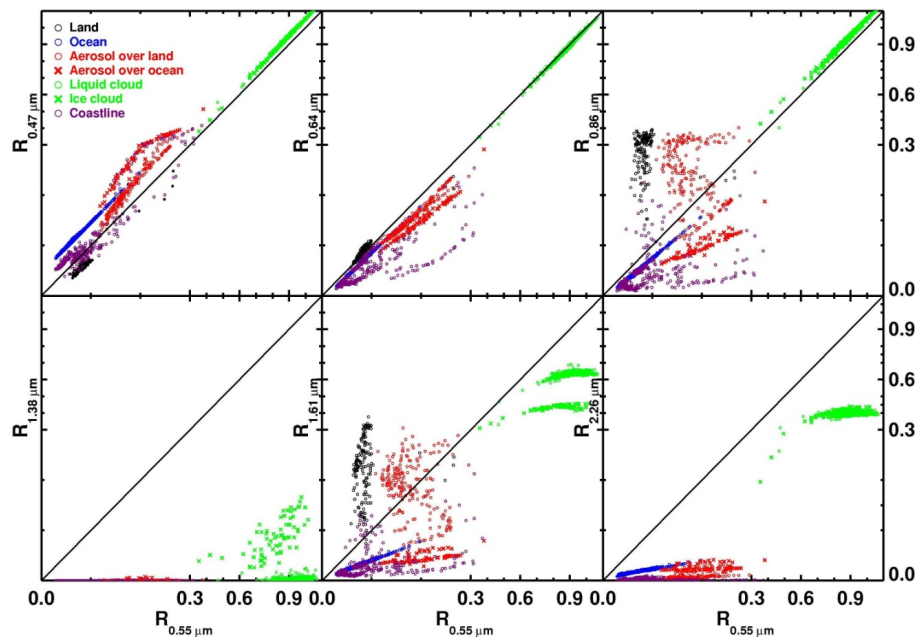


Fig. 6c. Same as in Fig. 6a, but on 25 March 2011.

Title Page

Abstract

Introduction

Conclusions

References

Tables

Figures

◀

▶

◀

▶

Back

Close

Full Screen / Esc

Printer-friendly Version

Interactive Discussion

Simulation of GOES-R ABI aerosol radiances using WRF-CMAQ:

S. A. Christopher

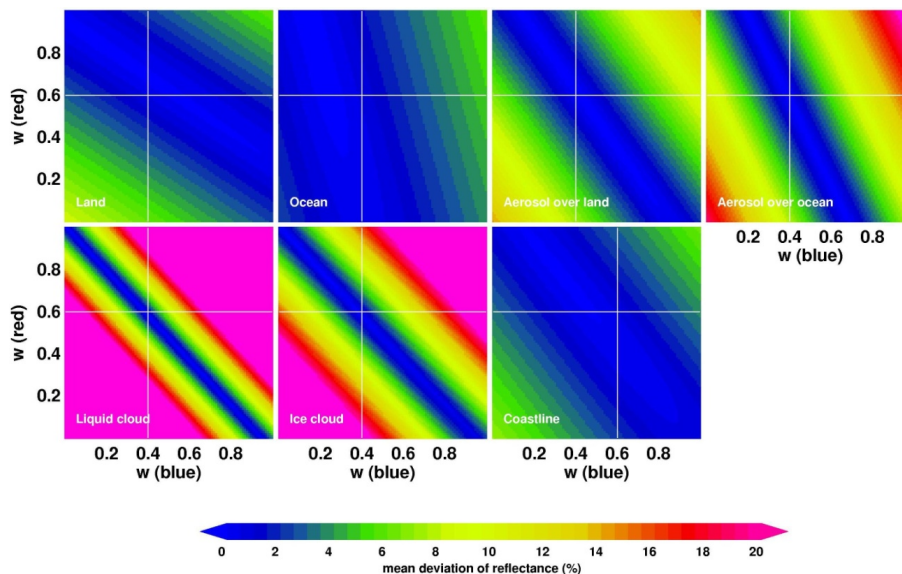


Fig. 7a. Mean difference between the synthesized and simulated green band reflectance with varying w_B and w_R for land, ocean, aerosol (over land and ocean), cloud (liquid and ice), and coastline for 10 June 2008. The unit is reflectance in percent. The point at $w_B = 0.4$ and $w_R = 0.6$ is shown for land, ocean, aerosol, and cloud. The point at $w_B = 0.6$ and $w_R = 0.6$ is also shown for coastline.

Simulation of
GOES-R ABI aerosol
radiances using
WRF-CMAQ:

S. A. Christopher

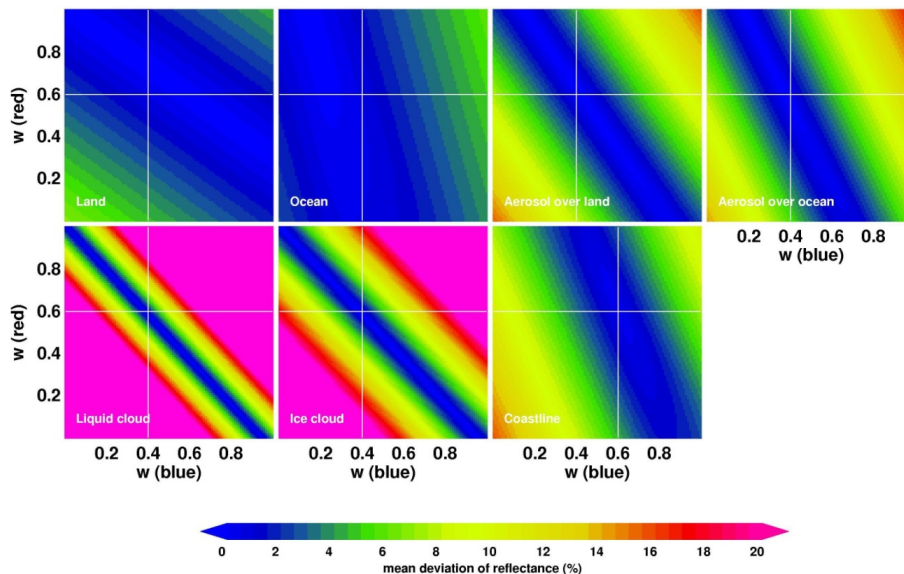


Fig. 7b. Same as in Fig. 7a, but for 8 July 2010.

Title Page

Abstract Introduction

Conclusions References

Tables Figures

⏪ ⏩

⏴ ⏵

Back Close

Full Screen / Esc

Printer-friendly Version

Interactive Discussion



Simulation of
GOES-R ABI aerosol
radiances using
WRF-CMAQ:

S. A. Christopher

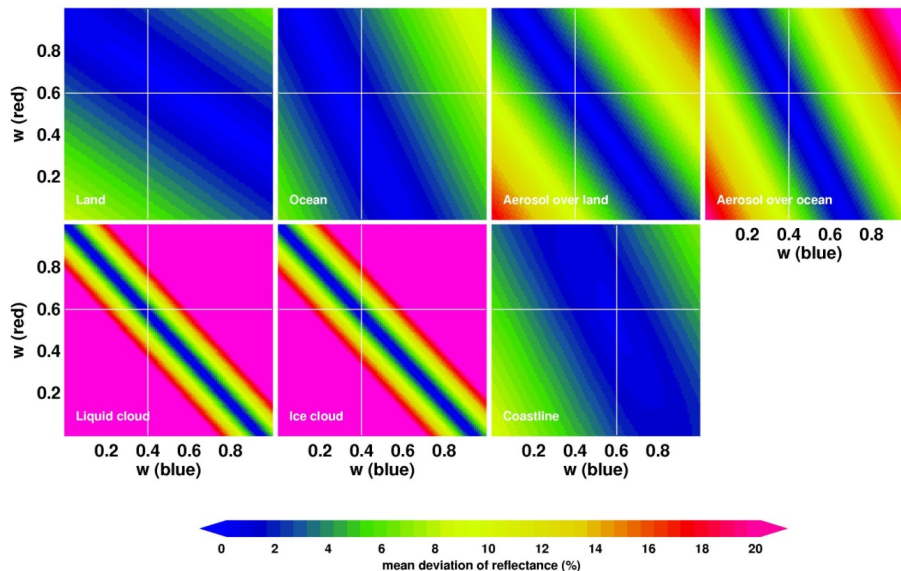


Fig. 7c. Same as in Fig. 7a, but for 25 March 2011.

Title Page

Abstract Introduction

Conclusions References

Tables Figures

⏪ ⏩

⏴ ⏵

Back Close

Full Screen / Esc

Printer-friendly Version

Interactive Discussion



Simulation of GOES-R ABI aerosol radiances using WRF-CMAQ:

S. A. Christopher

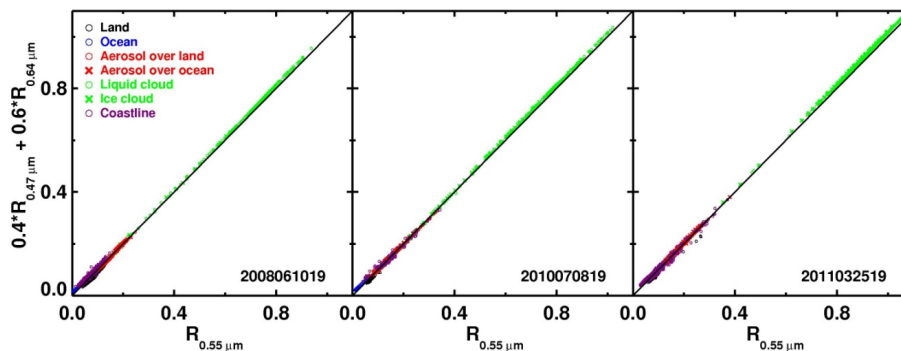


Fig. 8. Comparison of the synthesized and simulated green band reflectance, where the synthesized green band reflectance is derived from the blue and red band reflectance. The coastline are produced with a different blue-red combination such as $G_{\text{syn}} = 0.6 \cdot B + 0.6 \cdot R$.

Simulation of GOES-R ABI aerosol radiances using WRF-CMAQ:

S. A. Christopher

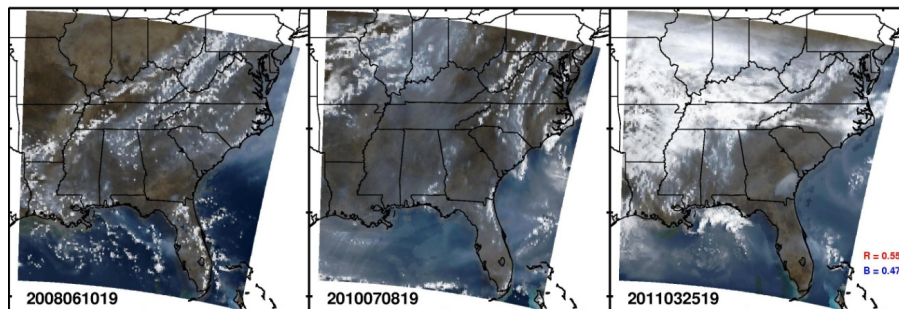


Fig. 9. Synthetic RGB imagery at 19:00 UTC, 10 June 2008 (left), 8 July 2010 (middle), and 25 March 2011 (right). The green band reflectance is synthesized from the simulated blue and red band reflectance using the relations, $G_{\text{syn}} = 0.4 \cdot B + 0.6 \cdot R$ for land, ocean, aerosol, and cloud, and $G_{\text{syn}} = 0.6 \cdot B + 0.6 \cdot R$ for coastline.

[Title Page](#)[Abstract](#)[Introduction](#)[Conclusions](#)[References](#)[Tables](#)[Figures](#)[◀](#)[▶](#)[◀](#)[▶](#)[Back](#)[Close](#)[Full Screen / Esc](#)[Printer-friendly Version](#)[Interactive Discussion](#)